IOP Publishing

Photocatalysts for Energy and Environmental Sustainability

Vijay B Pawade and Bharat A Bhanvase

Chapter 6

Photocatalysis for organic degradation using perovskite materials

Phuong Hoang Nguyen, Thi Minh Cao and Viet Van Pham

6.1 Introduction

In recent years, the issue of organic compound pollution, especially that caused by persistent organic pollutants (POPs), has become increasingly severe [1, 2]. These compounds are often used in producing various industrial products, leading to their widespread release into the environment. Organic compounds can be found in multiple water sources, including rivers, lakes, and groundwater. They can also enter the food chain through the consumption of contaminated water, causing harm to human and animal health [3]. In addition, long-term exposure to organic compounds can lead to a variety of health problems, including cancer, reproductive disorders, and immune system damage [4]. POPs and industrial chemicals that were manufactured in great quantities during the 20th century directly affect human and animal health. When examining the effects of pollution on morbidity and mortality in relation to other risk factors, the results indicate that pollution remains one of the most significant contributors to disease and premature death worldwide. According to figure 6.1, the number of deaths attributed to pollution is comparable to the number of deaths caused by smoking. This highlights the substantial and ongoing impact of pollution on global health outcomes. Exposure to high levels of persistent organic pollutants (POPs) can have detrimental health effects on both humans and animals. These effects are well documented and may include various adverse outcomes, such as cancer, nervous system damage, reproductive disorders, and immune system disruption. It is important to recognize that POPs have the potential to cause significant harm to living organisms, highlighting the need for effective measures to reduce exposure and mitigate their impact on health [5].

To address this issue, it is necessary to implement effective wastewater treatment processes in production facilities, enhance the monitoring and assessment of water quality to detect pollutants promptly, and implement other measures such as the use

doi:10.1088/978-0-7503-5697-8ch6

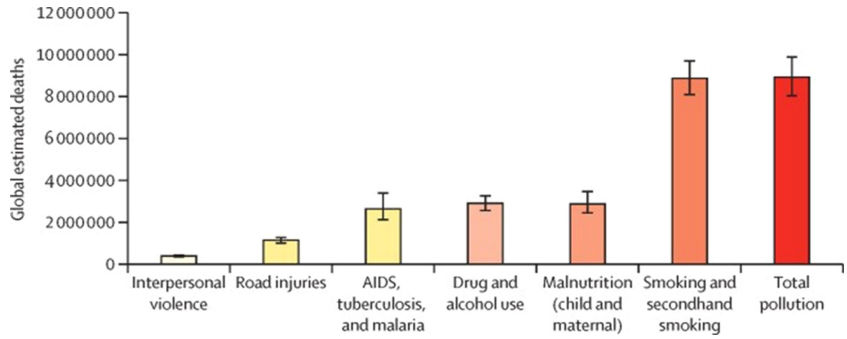

Figure 6.1. Global estimated deaths by major risk factor or cause. Reprinted from The Lancet [6], Copyright (2022), with permission from Elsevier.

of wastewater treatment technologies, a reduction in the chemicals used in production, and the use of recycled water sources. Furthermore, increasing education and awareness about environmental pollution is also critical in reducing pollution. Governments and nongovernmental organizations need to improve the information, education, and training offered to communities to raise awareness about environmental issues and enhance cooperation and consultation with businesses and organizations in implementing effective pollution reduction measures.

In terms of technical approaches, several methods can be used to reduce organic pollutants, which can be broadly categorized into prevention, treatment, and remediation approaches. For instance, biological treatment based on the use of microorganisms to degrade organic pollutants; physical and chemical treatment; phytoremediation; and adsorption. Therein, advanced oxidation processes (AOPs) can be employed to remove or degrade organic pollutants. These include activated carbon adsorption, advanced oxidation processes (e.g. ozonation, UV irradiation, photocatalysis, and chemical oxidation), air stripping, and membrane filtration. Among advance oxidation methods, photocatalysis and other processes based on photocatalysis, i.e. the photo-Fenton method, the use of a peroxymonosulfate (PMS) activator, etc. are promising technologies for the treatment of water contaminated with organic compounds. These processes use light to activate a photocatalyst, typically TiO_2, to generate highly reactive oxygen species that can degrade organic pollutants. One of the significant advantages of photocatalysis is that it is a green technology that does not require chemicals or produce harmful byproducts. In addition, photocatalysis can treat a wide range of organic contaminants, including pesticides, pharmaceuticals, and dyes. Furthermore, photocatalysis is a relatively simple and low-cost technology that can easily be scaled up for industrial applications. Overall, the use of photocatalysis in treating water contaminated with organic compounds offers several advantages over traditional treatment methods and shows great potential for widespread adoption in the future [7].

Perovskite materials have recently attracted significant attention in photocatalysis due to their unique optical and electronic properties [8]. These materials have a perovskite crystal structure that consists of a metal cation, an organic or inorganic

cation, and an anion. Perovskite materials have a high absorption coefficient, excellent charge carrier mobility, and long carrier lifetimes, which make them ideal for photocatalytic applications. Several studies have investigated the application of perovskite materials in photocatalysis to degrade organic pollutants, split water, and reduce carbon dioxide. For example, researchers have reported the successful use of perovskite materials in the photocatalytic degradation of organic dyes and the production of hydrogen gas from water [7]. These promising results suggest that perovskite materials have the potential to become a new class of photocatalysts for a wide range of environmental and energy applications.

This chapter provides a complete overview of the concept, properties, and application of perovskites as photocatalysts for organic pollutant removal. The primary methods used to synthesize perovskites are summarized in this chapter. In addition, this chapter describes some of the most important applications of perovskites in the photocatalysis field, including photocatalysis, the photo-Fenton reaction, and PMS activation for the degradation of organic pollutants in wastewater. Some conclusions and prospects are also briefly introduced, which could lead to breakthrough developments in perovskite materials design.

6.2 An overview of perovskite materials

6.2.1 An introduction to perovskites

Perovskites, named after Russian mineralogist Lev Perovski, are compounds with a crystal structure that follows the formula ABX_3, where A and B are cations and X is an anion (figure 6.2). The perovskite structure is a crystal structure that was first discovered in the mineral calcium titanate ($CaTiO_3$). It is characterized by a three-dimensional network of corner-sharing BX_6 octahedra that form a cubic lattice. The A cation occupies the center of the cube and is surrounded by octahedra.

The arrangement of the ideal perovskite structure can be described as follows:

$$(r_A + r_O) = \frac{\sqrt{2}}{2}A = \sqrt{2}(r_A + r_O), \tag{6.1}$$

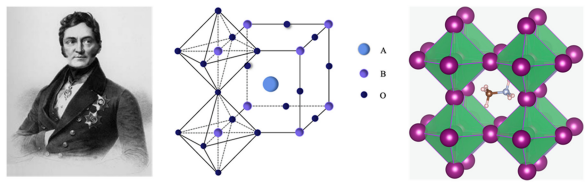

Figure 6.2. (a) Russian mineralogist Lev Perovski (1792–1856). This Count Lev Alekseevich Perovski image has been obtained by the author(s) from the Wikimedia website, where it is stated to have been released into the public domain. It is included within this book on that basis. (b) The structure of ABO_3 perovskite-type oxides. Reprinted from [10], Copyright (2021), with permission from Elsevier. (c) A methylammonium cation ($CH_3NH_3^+$) occupies the central A site, surrounded by 12 nearest-neighbor iodide ions in corner-sharing PbI_6 octahedra. Reproduced from [11]. CC BY 4.0.

where r_A, r_B, and r_O represent the ionic radii of the cations A and B and the anion O, respectively. Although the idealized structure is primitive cubic, differences in the sizes of the cations can cause distortions. This typically involves tilting of the octahedral units (known as octahedral tilting). The stability of the perovskite structure is described by a tolerance factor t, which represents the range of relative ionic sizes [3]:

$$t = \frac{(r_A + r_O)}{\sqrt{2}(r_B + r_O)}. \tag{6.2}$$

Empirically, if the tolerance factor is between 0.95 and 1.0, the structure is cubic. If $0.8 < t < 0.9$, the compound transforms into a tetragonal, rhombohedral, or orthorhombic crystal [9]. In photocatalytic studies, lattice distortion significantly affects the crystal field, altering dipoles and electronic band structures, which in turn impact the behaviors of photogenerated charge carriers, including excitation, transfer, and redox reactions, during the photocatalytic process.

Figure 6.3 shows that energy-dispersive x-ray (EDX) mapping of the elements in perovskite oxides ($BaTiO_3$ and $SrTiO_3$) exhibits visible particles on the particle clusters, and it also shows a uniform arrangement of Mo and S atoms on those clusters. $SrTiO_3$ and $BaTiO_3$ perovskite-type oxides offer a viable alternative to the predominantly used TiO_2 due to their favorable band positions, optical

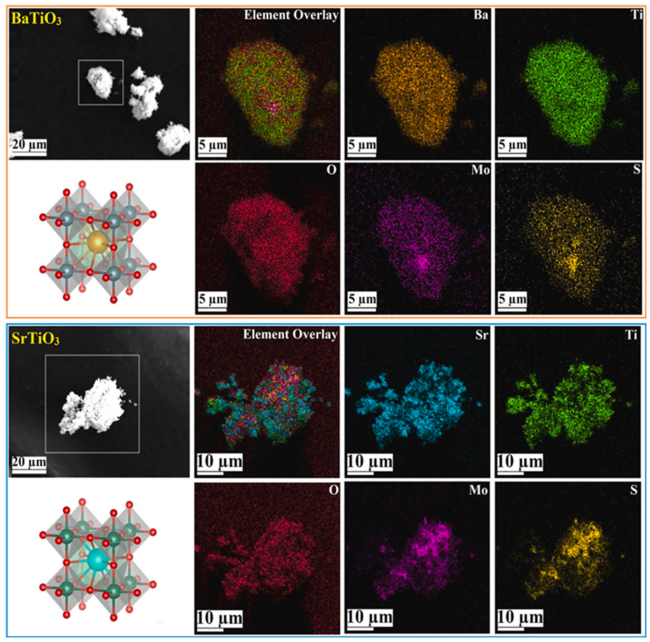

Figure 6.3. Elemental mapping images of photodeposited $BaTiO_3$ and $SrTiO_3$ nanocrystal clusters. Reprinted from [12], Copyright (2023), with permission from Elsevier.

characteristics, and crystallographic properties. These qualities make them suitable for effective photochemical energy conversion reactions.

In addition to the oxide-based perovskites, another type called 'perovskite halides' is a group of materials with the formula ABX_3, where A represents an organic and/or inorganic cation with a single oxidation state, B represents a group 4A metal with a valence of two (e.g. Pb^{2+}, Ge^{2+}, Sn^{2+}, etc.), and X corresponds to a halide anion, e.g. I^-, Cl^-, Br^-, etc [8]. These materials have gained tremendous attention due to their excellent optoelectronic properties, such as high light absorption coefficients, long carrier diffusion lengths, and high charge carrier mobilities.

In general, perovskites have shown great promise as low-cost and high-performance materials for solar cells. They have achieved remarkable power conversion efficiencies (PCEs) that exceed 25% and are comparable to the efficiencies of traditional silicon solar cells. In addition to their use in photovoltaics, metal halide perovskites have also been investigated for use in other optronics applications (light-emitting diodes (LEDs), photodetectors, photodiodes, and lasers). Overall, metal halide perovskites represent a promising class of materials with significant potential for advancing the field of solar energy and optoelectronics. Ongoing research and development efforts aim to address their stability issues and further enhance their performance for practical applications.

The bandgap energy of halide perovskites is one of the important factors that affect their optical properties. The bandgap is the energy required to push an electron from the valence band (VB) to the conduction band (CB), creating an electron–hole pair. The smaller the bandgap, the greater the semiconductor's ability to absorb light. Figure 6.4 shows the bandgaps of oxide-type perovskites (a) and halide-type perovskites (b) with the redox levels for the formation of reactive oxygen species (ROS) and $OH^{\bullet}$ radicals. For organic–inorganic perovskites ($MAPbI_3$), research studies have observed a small bandgap (about 1.5 eV) and a high light absorption coefficient of 105 cm^{-1} [13]. This means that $MAPbI_3$ one μm thick can absorb all light with a wavelength shorter than 800 nm in the solar spectrum. Moreover, by modifying factors such as size, composition substitution, phase segregation, phase transition, and deformation, it is possible to extensively adjust the range of light absorption in perovskite halides from UV to near-infrared wavelengths. The halogen anions that appear in the chemical formula $APbX_3$ for halide perovskites affect their CB energy levels. For instance, the bandgap of $MAPbI_3$ can be extensively tuned simply by changing the ratio of the different halogen ions. Similarly, continuous tuning of the spectrum can be achieved in inorganic halogen perovskites, as shown, for example, by $CsPbBr_3$, whose bandgap can be tuned from 1.88 to 3.03 eV by partially replacing Br with Cl or I. Furthermore, perovskite halides are a group of materials with unique photocatalytic properties. Their CBM and VBM positions are suitable for promoting many photocatalytic reactions [13].

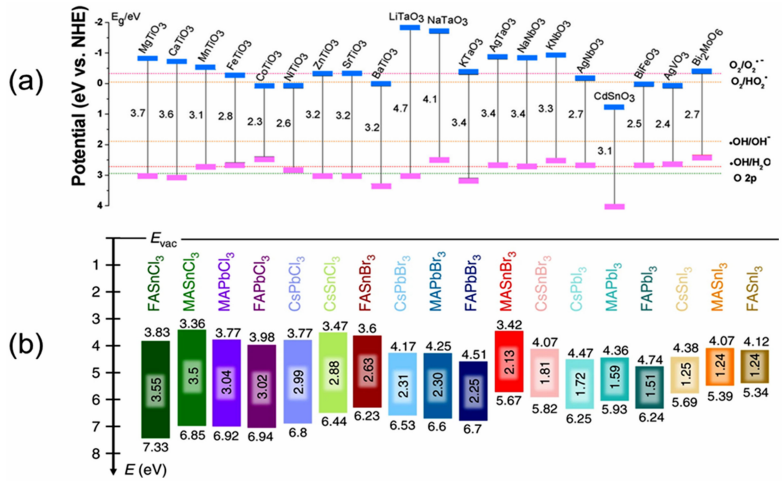

Figure 6.4. (a) E_g values (in eV) and the positions of the CB (upper) and the VB (lower) for various perovskite semiconductors at a pH of 7 vs. normal hydrogen electrode (NHE). Reprinted from [14], Copyright (2019), with permission from Elsevier. (b) A schematic energy level diagram of the 18 metal halide perovskites. Reproduced from [15]. CC BY 4.0.

6.2.2 The properties of perovskites

Perovskites have many advantageous properties for photovoltaics and photocatalysis due to their outstanding properties (figure 6.5).

6.2.2.1 Optoelectronic properties

Perovskite materials exhibit exceptional optoelectronic properties, making them suitable for various applications. Deschler *et al* [16] investigated the optoelectronic properties of perovskite materials and demonstrated that perovskite materials possess a high absorption coefficient, enabling efficient light harvesting across a wide spectrum, including visible and near-infrared wavelengths. In addition, they observed efficient charge transport due to long carrier diffusion lengths in these materials, making them suitable for application in solar cells and photocatalysis [17].

6.2.2.2 Tunable bandgap

Perovskite materials have quite diverse bandgap values that range from 2.1 to 4.0 eV (table 6.1) and a specific crystal structure that corresponds to a three-dimensional arrangement of metal cations, such as lead (Pb), tin (Sn), or other elements, surrounded by an octahedral arrangement of oxygen anions. Perovskite materials possessing the ABO_3 structure offer numerous benefits that make them a highly promising option for photocatalysis. These advantages include straightforward synthesis methods, adjustable physicochemical properties, well-suited frameworks, diverse levels of lattice distortion, and localized sites for surface oxidation and reduction reactions. These characteristics contribute to their potential to be excellent choices for photocatalytic processes.

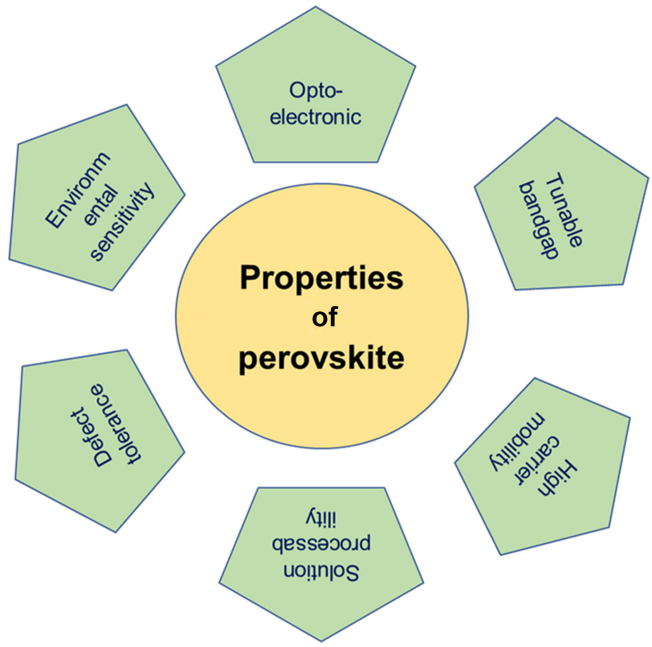

Figure 6.5. Some properties of perovskites.

Table 6.1. The bandgaps of some perovskite materials. Reproduced from [19]. CC BY 4.0.

Material	Bandgap (eV)
$SrTiO_3$	3.20
$NaTaO_3$	4.00
$CaTiO_3$	3.62
$BiFeO_3$	2.40
$LaFeO_3$	2.00
$NaNbO_3$	3.48
$LaCoO_3$	2.10
Bi_2WO_6	2.70
$La_2Ti_2O_7$	3.28

One of the remarkable features of perovskite materials is their tunable bandgap, which can be adjusted to absorb light across a wide range of energies. This tunability is advantageous for applications such as solar cells and light-emitting devices. Prasanna *et al* synthesized and investigated [18] tin and lead iodide perovskite semiconductors with the composition AMX_3, where M is a metal and X is a halide. The introduction of a smaller A-site cation into a perovskite structure can induce two distinct distortions: tilting of the MX_6 octahedra or isotropic

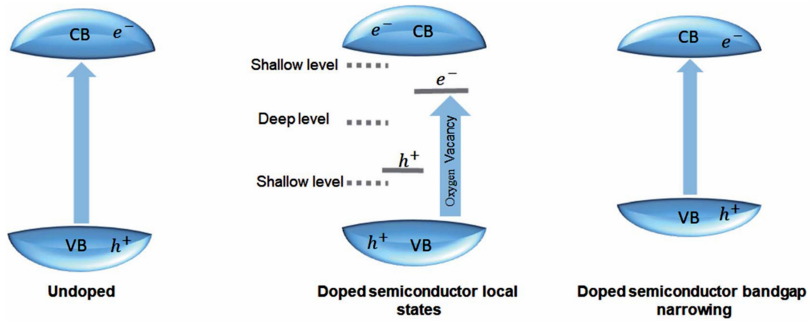

Figure 6.6. The effect of doping on the bandgap. Reproduced from [19]. CC BY 3.0.

contraction of the lattice. The former effect generally increases the bandgap, while the latter decreases it. In the case of lead iodide perovskites, replacing the larger formamidinium cation with the smaller cesium cation resulted in an expanded bandgap, which was attributed to octahedral tilting. Conversely, tin-based perovskites, being slightly smaller than lead, displayed no octahedral tilting upon cesium substitution but rather lattice contraction, leading to a progressive reduction in the bandgap. This study demonstrated a systematic approach to fine-tuning the bandgap and band positions of metal halide perovskites by controlling the cation composition. This research also showcased the development of solar cells that have bandgaps optimized for harvesting infrared light at up to 1040 nm, achieving a stabilized power conversion efficiency of 17.8%. The findings provide insights into cation-based bandgap tuning in 3D metal halide perovskites and have implications for the development of perovskite semiconductors for optoelectronic applications [18].

In addition, the control of the band positions and bandgaps of perovskites is also of interest in the visible-light-driven photocatalysis field. Figure 6.6 shows the effects on the bandgap of perovskites of doping to form new states, i.e. shallow and deep levels or oxygen vacancy states. Besides, the narrow bandgap of perovskites helps them become more effective in photocatalytic reactions under visible light conditions.

6.2.2.3 High carrier mobility

Perovskite materials exhibit high charge carrier mobility, allowing efficient movement of electrons and holes through the material. This high mobility is crucial to obtain high-performance electronic and optronics devices. Liu *et al* [20] synthesized InP and InAs nanocrystals (NCs) and used various inorganic ligands (molecular metal chalcogenide complexes (MCCs) and chalcogenide ions to cap the NCs). These inorganic ligands effectively replaced the organic ligands on the NC surfaces and stabilized the colloidal solutions of InP and InAs NCs in polar solvents. Moreover, they facilitated efficient charge transport between individual NCs. The films of InP and InAs NCs capped with MCCs exhibited high electron mobility, with $Cu_7S_4^-$ MCC ligands achieving electron mobility exceeding 15 $cm^2\ V^{-1}\ s^{-1}$. In addition, Lim *et al* [21] observed similar long-range mobilities of 0.3 to 6.7 $cm^2\ V^{-1}\ s^{-1}$ in perovskites such as $FA_{0.83}Cs_{0.17}Pb(I_{0.9}Br_{0.1})_3$, $(FA_{0.83}MA_{0.17})_{0.95}Cs_{0.05}Pb(I_{0.9}Br_{0.1})_3$, and

$CH_3NH_3PbI_{3-x}Cl_x$ polycrystalline films, highlighting their potential for use in various optoelectronic applications in which efficient charge transport is crucial.

6.2.2.4 Processability in solution

Perovskite materials can be processed in solution, which offers advantages for large-scale manufacturing processes. They can be deposited using techniques such as spin-coating, inkjet printing, or spray coating, enabling the fabrication of thin films with good uniformity and low-cost manufacturing potential. A study by Hu focused on scaling up perovskite photovoltaic technology through the exploration of film formation, device architectures, deposition methods, and scalable manufacturing approaches. This study emphasized the importance of precise control over nucleation and crystal growth during the film formation process to achieve high-performance perovskite solar cells [22].

6.2.2.5 Defect tolerance

Perovskite materials show a certain degree of tolerance toward defects, which can be beneficial for photocatalytic performance. Defects in the crystal structure can trap charge carriers, reducing their mobility. However, in perovskites, these trapped carriers can be released and continue to contribute to the device's functionality. Steirer *et al* [23] explored the defect tolerance characteristic of perovskite materials, with a specific focus on methylammonium lead triiodide ($MAPbI_3$) perovskite, and indicated that defects in the crystal structure influenced the performance and stability of energy-related devices utilizing this material. Furthermore, MAPbI3 perovskite exhibited a certain level of tolerance towards specific defects in its crystal structure. These defects have the potential to trap charge carriers, resulting in a decrease in their mobility. However, perovskite materials possess the capability to release these trapped charge carriers, enabling them to continue contributing to the device's overall performance [24].

Defect engineering provides a convenient and effective approach for improving the photocatalytic efficiency of perovskite materials. The substitution of different materials can introduce defects into the perovskite structure. These defects serve as sites that can trap charge carriers, leading to enhanced charge separation and increased photocatalytic efficiency. In addition, the existence of the intrinsic factors, e.g. Sn^{4+} that are easy formation of Sn vacancies, impacting to the defect chemistry and subsequent recombination of charge carriers, prolonged exposure of these materials to extrinsic factors (e.g., air, O_2) can severely degrade their key optoelectronic properties [17].

6.2.2.6 Environmental sensitivity

Perovskite materials can be sensitive to moisture, heat, and light exposure. They tend to degrade in the presence of moisture and are susceptible to thermal stress. However, ongoing research aims to improve their stability and durability for practical applications. Ahangharnejhad *et al* presented a method for protecting metal halide perovskite solar cells from degradation in high-humidity environments using a sputtered SiO_2 barrier coating. The SiO_2 protective layer significantly

enhanced the devices' resistance to extreme humidity conditions, increasing their lifetimes by approximately 60 times for $CH_3NH_3PbI_3$ and around 600 times for triple-cation perovskite material. Real-time laser-beam-induced current (LBIC) measurements validated the effectiveness of this approach in preventing degradation at the edges of scribed lines, making it suitable for the production of monolithically integrated modules [25].

6.3 Methods used to synthesize perovskite materials

There are several methods for making perovskite materials, i.e. wet chemical methods (sol–gel process hydrothermal route, coprecipitation method, electrochemical synthesis, and emulsion or microemulsion synthesis, etc.), solid-state reaction methods, template-assisted methods, etc. These methods can be adjusted to control the properties of the perovskite material, such as its crystal structure, morphology, and surface area, which can affect its photocatalytic activity [26].

6.3.1 Wet chemical methods

Wet chemical synthesis, also known as solution-based synthesis, is a broad term that refers to a wide range of chemical processes used to create or modify materials in a liquid or dissolved form. It involves the reaction of chemical precursors dissolved in a solvent to form a desired product. The reaction can be carried out at various temperatures, pressures, and reaction times, depending on the specific synthesis requirements. The reactants may undergo various chemical transformations, such as precipitation, hydrolysis, redox reactions, or complexation, to form the desired product. Wet chemical synthesis is widely used in various fields, including chemistry, materials science, nanotechnology, and pharmaceuticals. It offers several advantages, such as simplicity, scalability, and the ability to control the composition, size, shape, and structure of the resulting materials.

6.3.1.1 The sol–gel method

The sol–gel technique is commonly used to prepare nanosized perovskites with a high surface area. It involves the mixture of precursor compounds in specific solvents to form a stable 'sol,' which is then transformed into a gel-like system (both liquid and solid phases). The gel is then dried to evaporate the solvent and undergoes heating to obtain the desired perovskite materials [27]. Parida *et al* [28] synthesized $LaFeO_3$ perovskite nanomaterials using the sol–gel method at 130 °C. This heating process caused changes in the color and viscosity of the sol. When further heated, the brown, porous dry gel automatically ignited due to the thermal redox reaction. Finally, a solid was created by a self-burning process and then activated at different temperatures (500 to 900 °C) for 2 h to obtain a visible-light photocatalytic material. Wang *et al* [29] prepared perovskite materials including $La(NO_3)_3$ and $B(NO_3)_2$ (B = Mn, Fe, Co, Ni, Cu, Zn) by a sol–gel method using an ethylene glycol and alcohol mixture as a complex. In general, this synthesis method is quite simple: drying at 100 °C and annealing and sintering processes (500 °C–700 °C) were performed to obtain the final product.

6.3.1.2 *The hydrothermal method*

The hydrothermal method is one of the standard techniques used to synthesize perovskite particles with controlled shapes. This method subjects a reaction mixture to high-temperature and -pressure conditions in a stainless steel autoclave, and the final product is collected after cooling. Zhao *et al* [30] synthesized $CaTiO_3$ particles with a controlled morphology. Their study pointed out that rectangular $CaTiO_3$ particles exhibited the highest photocatalytic activity for the degradation of methylene blue under UV irradiation due to their high specific surface area compared to the surface areas of cubic and spherical particles.

6.3.1.3 *The coprecipitation method*

The coprecipitation method is another important technique used to synthesize perovskite materials. It is conducted using a suitable precipitating agent to coprecipitate two or more precursor components homogeneously [31]. Moshtaghi *et al* synthesized $CaSnO_3$ nanocubes using a simple and green coprecipitation method [32]. To obtain the final product, $CaSnO_3$, the researchers utilized a complex precursor called $Ca(sal)_2$ as a calcium source and $SnCl_2$ as a source of tin. The synthesis procedure employed water as an environmentally friendly solvent, and various alkaline agents were used as precipitating agents. After the reaction, the resulting precipitate was subjected to centrifugation, followed by washing and drying. Subsequently, the obtained material was annealed at a temperature of 900 °C for 5 h. Using this process, the researchers successfully obtained the desired final product, $CaSnO_3$. Junwu *et al* [33] synthesized $LaCoO_3$ nanocrystals using the coprecipitation method, in which NaOH was used as the precipitating agent. After precipitation, the resulting precipitates were centrifuged, washed, and dried at 100 °C. The dried residue was then annealed at 600 °C to obtain the product.

Figure 6.7 illustrates the general method of precipitation synthesis. The precursors A and B are dissolved in solvents and then precipitated using a NaOH solution

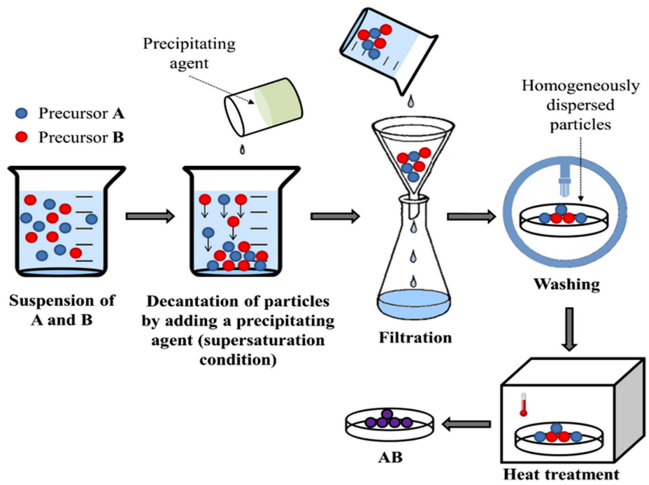

Figure 6.7. A general schematic of the coprecipitation method of perovskite preparation. Reprinted from [31], Copyright (2016), with permission from Elsevier.

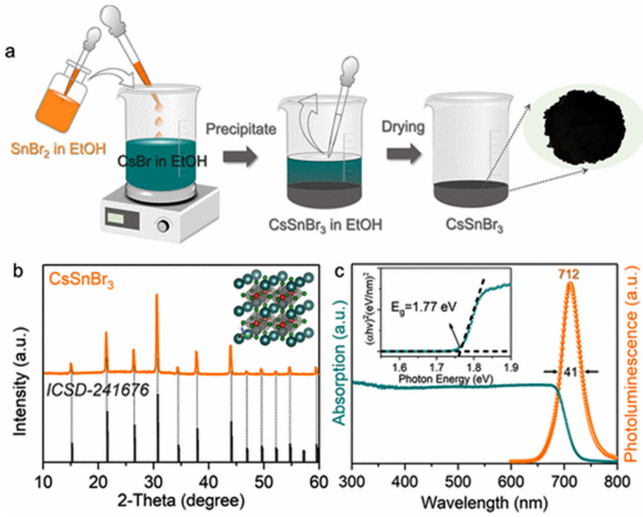

Figure 6.8. (a) A schematic of the coprecipitation process used to prepare $CsSnBr_3$ perovskite. (b) The x-ray diffraction pattern of $CsSnBr_3$. (c) The UV–vis absorption and PL spectra of $CsSnBr_3$. Reprinted with permission from [34]. Copyright (2023) American Chemical Society.

in water. The resulting precipitates are formed, filtered, and washed. Finally, the particles are annealed at a high temperature to form the final product.

Figure 6.8 represents a stepwise coprecipitation strategy for the synthesis of a stable $CsSnBr_3$ perovskite by a facile and low-cost strategy at room temperature [34]. Herein, ethanol as the solvent and salicylic acid as the additive were proposed for the synthesis of a $CsSnBr_3$ perovskite with a highly stable cubic phase. The results showed that the use of the ethanol solvent and the salicylic acid additive can not only effectively prevent the oxidation of Sn^{2+} during the synthesis processes but also stabilize the synthesized $CsSnBr_3$ perovskite. The absorption properties of the perovskite film remained consistent, and its photoluminescent (PL) intensity was significantly preserved at around 69% even after being stored for ten days. This performance was superior to that of a bulk $CsSnBr_3$ perovskite film synthesized using the spin-coating method, which experienced a decrease in PL intensity to 43% after only 12 h of storage. Clearly, this method is an efficient route for the synthesis of perovskite materials at room temperature.

6.3.2 Biotemplate-supported synthesis

The family of microorganisms provides various biological templates that can be used as an inspiration for designing and synthesizing various perovskite materials with different micro- and nanostructures and enhanced specific surface area. Different biological samples, such as algae, bacteria, fungi, viruses, etc. can be used, which offer the benefits of fast growth with control over the material's shape, size, and structure. In addition, biological materials, such as plant leaves, microorganisms, etc. provide good

templates for the development of materials, and the unique 3D designs of these samples can be mimicked in the desired materials [26].

Figure 6.9 depicts the introduction of a small quantity of the precious metal Pt into $LaNiO_3$, leading to the formation of $LaNi_{1-x}Pt_xO_3$ with a perovskite structure. In this process, Pt is dispersed atom by atom within the crystal lattice of the perovskite and is supported on SiO_2 which has a high specific surface area. After reduction, the resulting product is $Pt/LaNiO_3/SiO_2$. This approach enables Pt to be incorporated into the perovskite lattice, resulting in a uniform dispersion of Pt atoms at the atomic level. In addition, there is a strong interaction between the Pt atoms and the perovskite material, which effectively prevents the sintering of the Pt atoms [35].

The advantages and disadvantages of the methods used to synthesize perovskite materials, including physical and chemical methods, are listed in table 6.2.

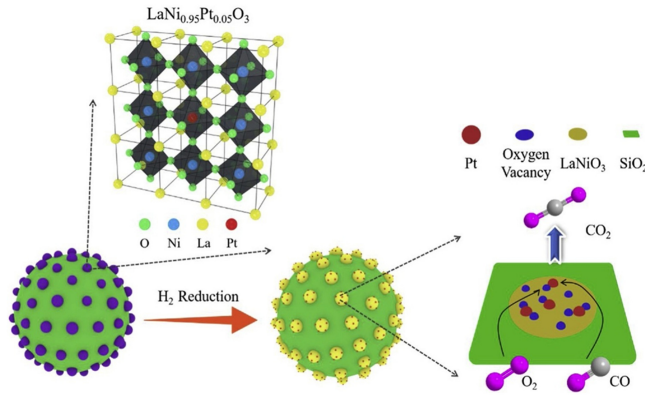

Figure 6.9. A schematic illustration of a process used to load highly dispersed Pt on $LaNiO_3$ which is on the surface of SiO_2 by reducing $LaNi_{1-x}Pt_xO_3/SiO_2$. Reprinted from [35], Copyright (2020), with permission from Elsevier.

Table 6.2. A summary of the advantages and disadvantages of common perovskite synthesis methods. Reprinted from [36], Copyright (2022), with permission from Elsevier.

Synthesis methods	Synthesis sub methods	Advantages	Disadvantages
Physical	High-temperature treatment	• Highly scalable • Simple	• Irregular and nonuniform morphology • Difficult to obtain single-phase and complex perovskites • Generally low specific surface area • High energy consumption
	• Mechanochemical • Reaction	• Highly scalable • Simple	• Difficult to control the morphology • Difficult to obtain single-phase and complex perovskites • High energy consumption

(*Continued*)

Table 6.2. (*Continued*)

Synthesis methods	Synthesis sub methods	Advantages	Disadvantages
	Radiation	• Short crystallization time • Produces uniform perovskite	• High energy consumption • Requires specialized instrument
Chemical	Coprecipitation	• Highly scalable • Simple	• Generally low crystallinity without additional post-treatment
	Sol–gel	• Highly scalable • Homogeneous and tunable morphology • Mild conditions	• Complex synthesis route • May involve toxic chemicals
	Hydrothermal/ solvothermal	• Homogeneous and tunable morphology	• Requires high temperature and pressure • May involve toxic chemicals

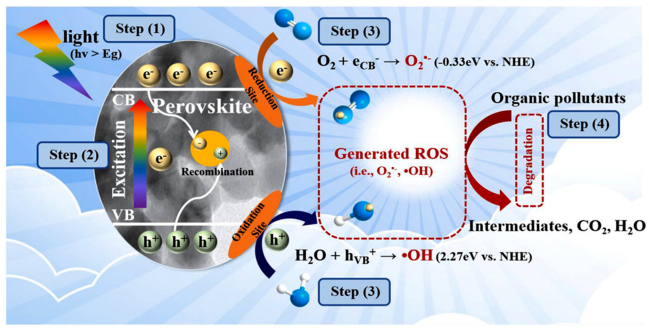

Figure 6.10. The mechanism of ROS production and pollutant degradation performed by perovskite photocatalysts. Reprinted from [10], Copyright (2021), with permission from Elsevier.

6.4 Perovskite photocatalysts for organic degradation

Perovskite-based photocatalytic agents are considered to be good candidates for the effective removal of organic pollutants from wastewater. Recently, many studies have focused on improving their strengths, enhancing the stability of perovskites, improving quantum efficiency, etc [37–40]. Figure 6.10 displays the photocatalytic processes of perovskites, in four steps: (i) light energy interacts with the perovskite material with the requirement that the energy of irradiation must be greater than E_g of the semiconductor. (ii) This activates electrons in the VB region of the

semiconductor, causing them to jump to the CB. This process leaves behind positive charges in the VB, which are called holes (h^+). These charges are key factors in carrying out the oxidation (h^+) and reduction reactions (e^-) in photocatalysis. (iii) Complex chemical reactions occur, creating components with strong reducing and oxidizing properties, such as $^{\bullet}OH$ and $^{\bullet}O_2^-$. (iv) Reactive radicals degrade the organic pollutants to form the intermediates CO_2 and H_2O (step 4).

The photocatalytic activities of selected perovskite-based and P25 photocatalysts for the degradation of organic dyes are listed in table 6.3.

6.4.1 Photocatalysis

As mentioned above, materials made from perovskites can absorb solar energy to create oxidizing sites (electron acceptors) and reducing areas (electron donors) for the purpose of oxidating organic pollutants into CO_2, H_2O, and other oxoanions. In photocatalytic degradation, photogenerated holes (h^+) can directly oxidize organic compounds into various intermediates or CO_2 and H_2O. Generally, OH^- derived from adsorbed H_2O is oxidized to hydroxyl radicals ($OH^{\bullet}$) by transferring h^+ from organic compounds to CO_2 and H_2O. Equations (6.3)–(6.5) describe the photocatalytic degradation reactions of organic compounds:

$$\text{Organic} + h^+ \rightarrow \text{intermediates}/CO_2 + H_2O \tag{6.3}$$

$$h^+ + OH^- \rightarrow OH^{\bullet} \tag{6.4}$$

$$\text{Organic} + OH^{\bullet} \rightarrow CO_2 + H_2O \tag{6.5}$$

However, the introduction of O_2 can inhibit the recombination of h^+ and e^- by forming $^{\bullet}O_2^-$ radicals, which then further protonate to form hydroperoxyl radicals ($^{\bullet}HO_2$) and subsequently hydroperoxide (H_2O_2), as depicted in equations (6.6)–(6.9):

$$(O_2)_{ads} + e^- \rightarrow {}^{\bullet}O_2^- \tag{6.6}$$

$$O_2 + OH \rightarrow HOO \tag{6.7}$$

$$HOO + e^- \rightarrow {}^{\bullet}HO_2^- \tag{6.8}$$

$$^{\bullet}HO_2^- + H^+ \rightarrow H_2O_2 \tag{6.9}$$

Figure 6.11 illustrates the use of a hybrid material based on a lead-free halide perovskite which is activated by light. This hybrid material exhibits enhanced photoelectrical effects and utilizes synergistic surface activation mechanisms. As a result, it supports an efficient process for converting aromatic C(sp3)–H bonds under visible light and in the presence of air.

Table 6.3. The photocatalytic activity of selected perovskite-based and P25 photocatalysts for the degradation of organic dyes [41].

Photocatalyst	BG (eV)	Dye type and/or concentration	Degradation rate ($1 - C/C_0$, %)	Catalyst loading	Light type	Preparation method
P25	3.2	RB, 20 μmol l^{-1}	3	5 g l^{-1}	$\lambda > 400$ nm	Commercial
$LaFeO_3$(500)			24			Sol–gel
$LaFeO_3$(600)			16			
$LaFeO_3$(700)			13			
$LaFeO_3$(800)			9			
$LaFeO_3$ nanocubes	2.01	RB	76.81 at 180 min	1 g l^{-1}	$\lambda > 400$ nm	Hydrothermal
$LaFeO_3$ nanorods	2.05		88.36 at 180 min			
$LaFeO_3$ nanospheres	2.1		90.8 at 180 min			
P25	3.2		5.1 at 180 min			Commercial
$LaNiO_3$	2.26	MO, 10 mg l^{-1}	74.9 at 5h	2 g l^{-1}	$\lambda > 400$ nm	Sol–gel
$CeCo_{0.05}Ti_{0.95}O_{3.97}$	1.57	Nile blue, 30 ppm	91 at 3h	3 g l^{-1}	254–310 and 410–500 nm	Sol–gel
$NaTaO_3$	4.13	MB, 2×10^{-4} mol l^{-1}	60 at 200 min	50 mg	$\lambda > 420$ nm	Hydrothermal
2.47 mol% Cr-doped $NaTaO_3$	3.95		70 at 200 min			
6.35 mol% Cr-doped $NaTaO_3$	3.28		~35 at 200 min			
P25	3.2	RB, 5×10^{-6} mol l^{-1}	75 at 150 min	2 g l^{-1}	$\lambda > 400$ nm	Commercial
$K_2La_2Ti_3O_{10}$	3.63		10 at 150 min			Steady-state reaction (SSR)
N-$K_2La_2Ti_3O_{10}$	3.59		20 at 150 min			SSR + NH_3 gas
CN-$K_2La_2Ti_3O_{10}$	2.92		90 at 150 min			SSR + urea
P25	3.2	MO, 0.02 g l^{-1}	~6 at 30 min	0.8 g l^{-1}	$\lambda > 400$ nm	Commercial
$K_2La_2Ti_3O_{10}$	3.69		~2 at 30 min			SSR
N-$K_2La_2Ti_3O_{10}$	3.44		~30 at 30 min			SSR + NH_3 gas
$LaFeO_3$		MB, 10 mg l^{-1}	~50 at 90 min	0.5 g l^{-1}	$\lambda > 400$ nm	Reverse microemulsion
$La_{0.9}Ca_{0.1}FeO_3$			~80 at 90 min			

$La_2Ti_2O_7$		MO, 1×10^{-5} mol l^{-1}	~55 at 90 min	1 g l^{-1}	UV, λ = 254 nm	Polymeric complex
$La_{1.5}Pr_{0.5}Ti_2O_7$			~25 at 90 min			
$La_{1.5}Gd_{0.5}Ti_2O_7$			90 at 90 min			
$La_{1.5}Er_{0.5}Ti_2O_7$			~50 at 90 min			
$LaFeO_3$	2.36	MB, 10 mg l^{-1}	~100 at 90 min	2 g l^{-1}	$\lambda > 400$ nm	Microwave-assisted route
P25	3.2		20 at 90 min			Commercial
$LaFeO_3$	2.1	RB	490 at 180 min	1 g l^{-1}	$\lambda > 400$ nm	Hydrothermal
P25	3.2	MO, 10 mg l^{-1}	~85 at 100 min	0.2 g l^{-1}	UV	Commercial
$LaCoO_3$	2.07		~85 at 100 min			Surface-ion adsorption method
P25	3.2	MB, 10 mg l^{-1}	~85 at 100 min			Commercial
$LaCoO_3$	2.07		~85 at 100 min			Surface-ion adsorption method
KNb_3O_8	3.06	Acid red G, 50 mg l^{-1}	63.03 at 60 min	1 g l^{-1}	UV, λ = 253.7 nm	SSR
0.3 wt% Cu-doped KNb_3O_8			93.23 at 60 min			
2 wt% Cu-doped KNb_3O_8			83.92 at 60 min			

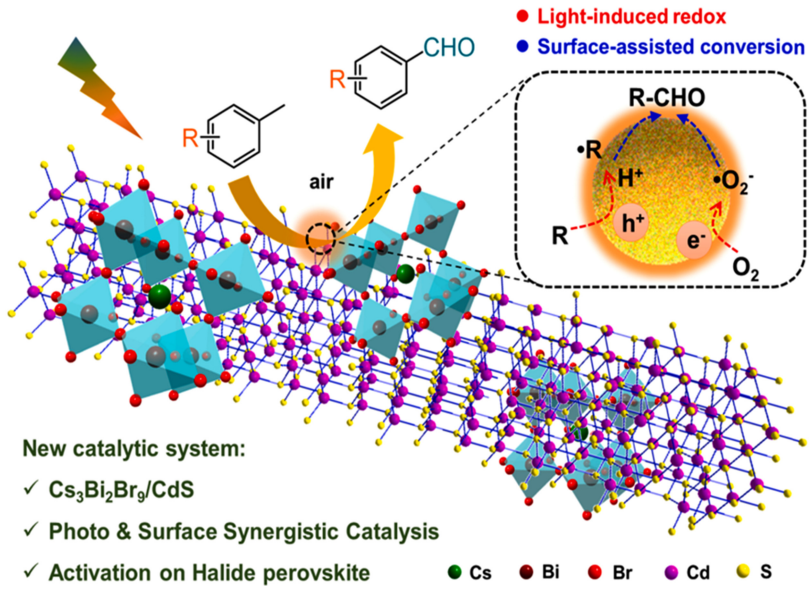

Figure 6.11. A schematic illustration of the photocatalytic conversion of aromatic C(sp3)–H bonds by a $Cs_3Bi_2Br_9$/CdS hybrid photocatalyst under air and visible light. The conversion involves the synergistic activation of photo and surface catalysis. Reprinted from [42], Copyright (2023), with permission from Elsevier.

6.4.2 Fenton and photo-Fenton catalysis

The Fenton and photo-Fenton processes are both AOPs that involve the generation of radicals for oxidation. The distinction between them lies in the origin of these radicals, as shown in figure 6.12. Therein, hydroxyl radicals ($^{\bullet}OH$) can be generated through the catalytic decomposition of hydrogen peroxide (H_2O_2) by ferric ions in the Fenton reaction. Meanwhile, the photo-Fenton reactions occur in the presence of UV or visible light, and the oxidative radicals derived from Fe^{3+}/H_2O_2 are produced through the action of the light source. In photocatalytic oxidation processes, electron–hole pairs are generated within the catalyst upon exposure to UV light, and the oxidative radicals are formed at the interface between the catalyst and water [43].

The Fenton method has attracted great interest due to its convenience and effectiveness. Notably, the Fenton method can produce many hydroxyl radicals ($^{\bullet}OH$) by introducing a divalent iron solution and hydrogen peroxide [44], as shown in equation (6.10).

$$Fe^{2+} + H_2O_2 \rightarrow Fe^{3+} + OH^- + OH^{\bullet} \tag{6.10}$$

The main result of the Fenton reaction, which is primarily governed by equation (6.10), is the formation of hydroxyl radicals ($HO^{\bullet}$). However, in the photo-Fenton process, two additional reactions occur simultaneously [45, 46]. First, there is the photolysis of hydrogen peroxide (H_2O_2) through the absorption of light energy ($h\nu$),

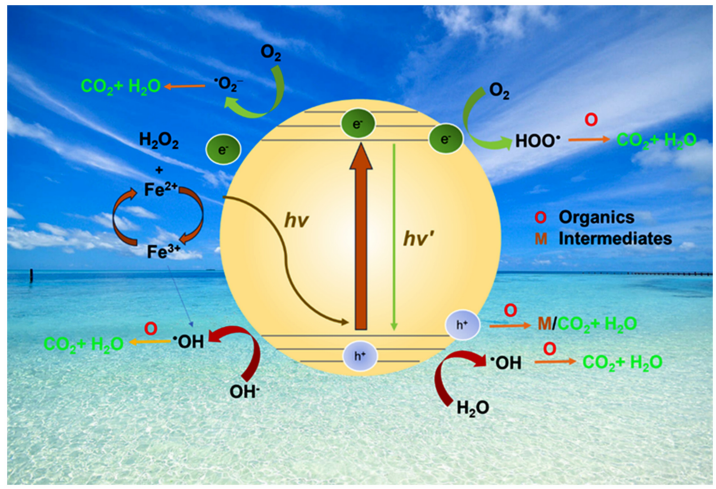

Figure 6.12. A schematic illustration of the photo-Fenton reactions of perovskites.

leading to the formation of two hydroxyl radicals ($HO^{\bullet}$) as shown in equation (6.11). This photolytic reaction occurs when H_2O_2 absorbs photons and undergoes a cleavage reaction, resulting in the generation of highly reactive hydroxyl radicals.

$$H_2O_2 \xrightarrow{hv} 2\ OH^{\bullet} \tag{6.11}$$

Second, there is the photoreduction of ferric ions (Fe^{3+}) in the presence of water (H_2O) and light energy ($h\nu$). This reaction, described by equation (6.11), involves the absorption of photons by Fe^{3+}, leading to the reduction of Fe^{3+} to ferrous ions (Fe^{2+}), the generation of hydroxyl radicals ($HO^{\bullet}$), and the release of a hydrogen ion (H^+). This photoreduction process contributes to the overall generation of hydroxyl radicals in the photo-Fenton process.

$$Fe^{3+} + H_2O \quad hv \quad Fe^{2+} + OH^{\bullet} + H^+ \tag{6.12}$$

Together, the Fenton reaction (equation (6.10)), the photolysis of H_2O_2 (equation (6.18)), and the photoreduction of Fe^{3+} (equation (6.11)) result in the production of hydroxyl radicals ($HO^{\bullet}$) in the photo-Fenton process. These highly reactive radicals play a crucial role in the degradation of organic pollutants by oxidizing and breaking down their chemical bonds.

6.4.3 PMS activation

PMS is frequently employed as an oxidizing agent in AOPs to generate sulfate radicals. These radicals can be activated through various methods. Instead of relying on energy-based activation methods such as solar/UV radiation, ultrasound, electricity, or heat, catalytic activation is more commonly employed. This is because it offers advantages such as lower cost and higher efficiency in decomposing PMS using transition-metal ions and heterogeneous catalysts. In AOP systems, the

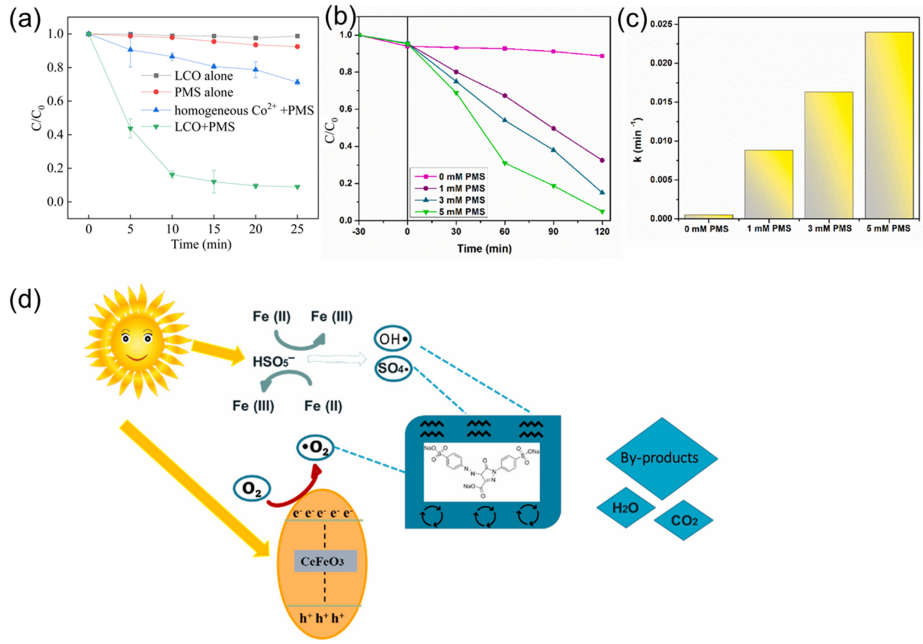

Figure 6.13. (a) BPA degradation in different reaction systems. Reaction conditions: [BPA] = 0.05 mM, [PMS] = 1.0 mM, [LCO] = 0.5 g l^{-1}, initial pH = 6.8. Reproduced from [47] with permission from the Royal Society of Chemistry. (b–c) Photocatalytic degradation curves of $CeFeO_3$ samples in the PMS/Vis system. (d) The proposed mechanism of the photoactivation of PMS over $CeFeO_3$ samples. Reprinted from [48], Copyright (2023), with permission from Elsevier.

presence of heterogeneous perovskite catalysts allows the generation of numerous ROS, including $HO^{\bullet}$ radicals, singlet oxygen, and $^{\bullet}O_2^-$. The activation of PMS by heterogeneous catalysts has gained significant attention because it enables easier separation of the catalysts, which helps to prevent secondary pollution issues that may arise in homogeneous systems.

Zhong *et al* synthesized La_2CoO_4+δ (LCO) perovskite and active PMS to degrade bisphenol A (BPA) [47]. As shown in figure 6.13a, LCO+PMS had a highly efficient photocatalytic performance, which was superior to those of LCO alone, PMS, or homogeneous Co^{2+}+PMS systems. Based on figures 6.13(b) and (c), it can be observed that the activity of bare PMS was relatively low, achieving only 12.6% degradation. This suggests that the activation of PMS on the surface of $CeFeO_3$ plays a more prominent role compared to light irradiation, which is illustrated in figure 6.13(c). Two primary interactions involving persulfate ions can be credited for the heightened activity observed in $CeFeO_3$/PMS/Vis systems. First, visible light can activate PMS, leading to its activation and the generation of reactive species. Second, the presence of ferrite sites within $CeFeO_3$ aids in the activation of PMS, facilitating the desired reactions. These interactions lead to the generation of free radicals, specifically sulfate radicals ($^{\bullet}SO_4^-$) and hydroxyl radicals

($HO^{\bullet}$), which are responsible for the decomposition of dye molecules. The proposed overall activation reactions are summarized in equations (6.13)–(6.15):

$$HSO_5^- + hv \rightarrow SO_4^{\bullet} + OH^{\bullet} \quad (6.13)$$

$$HSO_5^- + Fe(III) \rightarrow SO_5^{\bullet} + H^+ + Fe(II) \quad (6.14)$$

$$HSO_5^- + Fe(II) \rightarrow SO_4^{\bullet} + OH^{\bullet} + Fe(III) \quad (6.15)$$

Figure 6.13(c) shows that the visible-light photons are primarily absorbed by the surface of $CeFeO_3$ in the $CeFeO_3$/PMS/vis system. This absorption leads to the generation of photoexcited electrons in the conduction band and holes in the valence band of $CeFeO_3$. This $CeFeO_3$ can react with adsorbed oxygen molecules, leading to the formation of $^{\bullet}O_2^-$ radicals through a process known as electron transfer. These $^{\bullet}O_2^-$ radicals are highly reactive and can participate in subsequent oxidation reactions.

Simultaneously, PMS is also irradiated with light, resulting in the formation of sulfate radicals ($^{\bullet}SO_4^-$) and hydroxyl radicals ($^{\bullet}OH$). These radicals are generated through the activation of PMS by the absorbed light energy. The presence of PMS contributes to the overall radical generation in the system. In addition, the Fe^{3+} state within the $CeFeO_3$ perovskite structure can undergo oxidation, leading to the formation of additional radicals. This further enhances the photocatalytic oxidation processes occurring in the system.

Clearly, the combined action of $^{\bullet}O_2^-$ radicals, sulfate radicals, hydroxyl radicals, and other reactive species generated within the $CeFeO_3$/PMS/vis system contributes to the overall positive effect of the radicals. These radicals participate in various oxidation reactions, effectively degrading organic pollutants, such as dye molecules. Overall, the interplay between photoexcited electrons in $CeFeO_3$, $^{\bullet}O_2^-$ radicals and PMS activation through light irradiation results in the generation of a variety of radicals that drive the photocatalytic oxidation processes within the system, leading to the enhanced degradation of pollutants.

6.5 Conclusions

Perovskite materials possess exceptional crystallinity and unique features, making them highly promising as semiconductor photocatalysts for the degradation of organic pollutants. The ability to fine-tune their physicochemical properties by adjusting their chemical composition offers ample opportunities for developing novel nanocomposites. However, pristine perovskites suffer from limitations, i.e. low photocatalytic efficiency, poor stability, inadequate utilization of solar energy, rapid electron–hole recombination, and low redox potential. To overcome these challenges, researchers have capitalized on the flexibility of regulating perovskite properties to develop efficient photocatalysts for water remediation. Numerous perovskite-based nanocomposites have been synthesized and studied using various methods and strategies, including cationic substitution with dopants, downsizing and morphological modifications, and coupling with AOPs. While designing and preparing novel perovskite-based nanocomposites,

particularly through partial and full cationic substitution, is an elegant approach, it remains a challenging task.

The photocatalytic activity of perovskites is improved by controlling the bandgap, defects, morphology, etc. In addition, the photo-Fenton method and PMS activation by perovskite-based nanomaterials were discussed in this chapter. Perovskite-based nanomaterials have demonstrated encouraging outcomes as activators for PMS in applications. They have exhibited promising results in the removal of diverse organic pollutants, including endocrine disruptors, antibiotics, and dyes However, it is worth noting that metal halide perovskites face challenges related to their stability, especially in the presence of moisture and heat. To achieve broader success in practical applications utilizing perovskite-based nanomaterials, the following research directions have been identified:

(a) developing new perovskites and coupling perovskites with other semiconductors or metal nanoparticles;
(b) investigating the photocatalysis of realistic wastewater samples;
(c) upscaling perovskite catalysts;
(d) improving their stability and long-term performance to make them commercially viable;
(e) developing environmentally friendly synthesis methods;
(f) decorating 3D-printed materials with perovskite photocatalysts for use in industrial production, and
(g) improving catalyst separation (membrane filtration is commonly used for catalyst separation but using membranes for perovskite-based catalyst recovery can be costly and complex due to membrane fouling).

References

[1] Lomonaco T *et al* 2020 Release of harmful volatile organic compounds (VOCs) from photodegraded plastic debris: a neglected source of environmental pollution *J. Hazard. Mater.* **394** 122596

[2] Chaudhry G R and Chapalamadugu S J 1991 Biodegradation of halogenated organic compounds *Microbiol Rev.* **55** 59–79

[3] Singh S, Yadav R, Sharma S and Singh A N 2023 Arsenic contamination in the food chain: a threat to food security and human health *J. Appl. Biol. Biotechnol.* **11** 24–33

[4] Carpenter D O 2013 *Effects of Persistent and Bioactive Organic Pollutants on Human Health* (New York, NY: Wiley) DOI:10.1002/9781118679654

[5] Balk S J, Carpenter D O and Corra L *et al* 2010 *Persistent Organic Pollutants: Impact on Child Health* 9789241501101 World Health Organization Technical document

[6] Fuller R *et al* 2022 Pollution and health: a progress update *Lancet Planet. Health* **6** e535–47 (Corrected 18 May 2022 at https://doi.org/10.1016/S2542-5196(22)00145-0)

[7] Ahmed S *et al* 2011 Advances in heterogeneous photocatalytic degradation of phenols and dyes in wastewater: a review *Water, Air, Soil Pollut.* **215** 3–29

[8] Huang H, Pradhan B, Hofkens J, Roeffaers M B and Steele J A 2020 Solar-driven metal halide perovskite photocatalysis: design, stability, and performance *ACS Energy Lett.* **5** 1107–23

[9] Chen Z-Y, Huang N-Y and Xu Q 2023 Metal halide perovskite materials in photocatalysis: design strategies and applications *Coord. Chem. Rev.* **481** 215031
[10] Wei K, Faraj Y, Yao G, Xie R and Lai B 2021 Strategies for improving perovskite photocatalysts reactivity for organic pollutants degradation: a review on recent progress *Chem. Eng. J.* **414** 128783
[11] Eames C *et al* 2015 Ionic transport in hybrid lead iodide perovskite solar cells *Nat. Commun.* **6** 7497
[12] Kuru T *et al* 2023 Photodeposition of molybdenum sulfide on $MTiO_3$ (M: Ba, Sr) perovskites for photocatalytic hydrogen evolution *J. Photochem. Photobiol. A: Chem.* **436** 114375
[13] Luo J *et al* 2021 Halide perovskite composites for photocatalysis: a mini review *EcoMat* **3** e12079
[14] Kong J, Yang T, Rui Z and Ji H 2019 Perovskite-based photocatalysts for organic contaminants removal: current status and future perspectives *Catal. Today* **327** 47–63
[15] Tao S *et al* 2019 Absolute energy level positions in tin- and lead-based halide perovskites *Nat. Commun.* **10** 2560
[16] Deschler F *et al* 2014 High photoluminescence efficiency and optically pumped lasing in solution-processed mixed halide perovskite semiconductors *J. Phys. Chem. Lett.* **5** 1421–6
[17] Dey K, Roose B and Stranks S D 2021 Optoelectronic properties of low-bandgap halide perovskites for solar cell applications *Adv. Mater.* **33** 2102300
[18] Prasanna R *et al* 2017 Band gap tuning via lattice contraction and octahedral tilting in perovskite materials for photovoltaics *J. Am. Chem. Soc.* **139** 11117–24
[19] Irshad M *et al* 2022 Photocatalysis and perovskite oxide-based materials: a remedy for a clean and sustainable future *RSC Adv.* **12** 7009–39
[20] Liu W, Lee J-S and Talapin D V 2013 III–V nanocrystals capped with molecular metal chalcogenide ligands: high electron mobility and ambipolar photoresponse *J. Am. Chem. Soc.* **135** 1349–57
[21] Lim J *et al* 2022 Long-range charge carrier mobility in metal halide perovskite thin-films and single crystals via transient photo-conductivity *Nat. Commun.* **13** 4201
[22] Hu H *et al* 2020 Nucleation and crystal growth control for scalable solution-processed organic–inorganic hybrid perovskite solar cells *J. Mater. Chem.* A***8*** *1578–603*
[23] Steirer K X *et al* 2016 Defect tolerance in methylammonium lead triiodide perovskite *ACS Energy Lett.* **1** 360–6
[24] Farhad F T *et al* 2018 $MAPbI_3$ and $FAPbI_3$ perovskites as solar cells: Case study on structural, electrical and optical properties *Results Phys.* **10** 616–27
[25] Hosseinian Ahangharnejhad R *et al* 2021 Protecting perovskite solar cells against moisture-induced degradation with sputtered inorganic barrier layers *ACS Appl. Energy Mater.* **4** 7571–8
[26] Kumar A, Kumar A and Krishnan V J A c 2020 Perovskite oxide based materials for energy and environment-oriented photocatalysis *ACS Catal.* **10** 10253–315
[27] Salavati-Niasari M *et al* 2016 Synthesis, characterization, and morphological control of $ZnTiO_3$ nanoparticles through sol–gel processes and its photocatalyst application *Adv. Powder Technol.* **27** 2066–75
[28] Parida K, Reddy K, Martha S, Das D and Biswal N 2010 Fabrication of nanocrystalline $LaFeO_3$: an efficient sol–gel auto-combustion assisted visible light responsive photocatalyst for water decomposition *Int. J. Hydrog. Energy* **35** 12161–8

[29] Wang S *et al* 2018 Sol-gel preparation of perovskite oxides using ethylene glycol and alcohol mixture as complexant and its catalytic performances for CO oxidation *ChemistrySelect* **3** 12250–7
[30] Zhao H, Duan Y and Sun X 2013 Synthesis and characterization of $CaTiO_3$ particles with controlled shape and size *New J. Chem.* **37** 986–991,
[31] Athayde D D *et al* 2016 Review of perovskite ceramic synthesis and membrane preparation methods *Ceram. Int.* **42** 6555–71
[32] Moshtaghi S, Gholamrezaei S and Niasari M S 2017 Nano cube of $CaSnO_3$: facile and green co-precipitation synthesis, characterization and photocatalytic degradation of dye *J. Mol. Struct.* **1134** 511–9
[33] Junwu Z *et al* 2007 Solution-phase synthesis and characterization of perovskite LaCoO3 nanocrystals via a co-precipitation route *J. Rare Earths* **25** 601–4
[34] Cao L *et al* 2023 Highly ambient stable $CsSnBr_3$ perovskite via a new facile room-temperature 'Coprecipitation' strategy *ACS Appl. Mater. Interfaces* **15** 30409–16
[35] Zhang S *et al* 2020 SiO2 supported highly dispersed Pt atoms on $LaNiO_3$ by reducing a perovskite-type oxide as the precursor and used for CO oxidation *Catal. Today* **355** 222–30
[36] Koo P-L, Jaafar N F, Yap P-S and Oh W-D 2022 A review on the application of perovskite as peroxymonosulfate activator for organic pollutants removal *J. Environ. Chem. Eng.* **10** 107093
[37] Peng Y, Albero J and Garcia H 2019 Surface silylation of hybrid benzidinium lead perovskite and its influence on the photocatalytic activity *ChemCatChem* **11** 6384–90
[38] Schanze K S, Kamat P V, Yang P and Bisquert J 2020 Progress in perovskite photocatalysis *ACS Energy Lett.* **5** 2602–4
[39] Li Q and Lian T 2019 Ultrafast charge separation in two-dimensional CsPbBr3 perovskite nanoplatelets *J. Phys. Chem. Lett.* **10** 566–73
[40] DuBose J T and Kamat P V 2022 Efficacy of perovskite photocatalysis: challenges to overcome *ACS Energy Lett.* **7** 1994–2011
[41] Wang W, Tadé M O and Shao Z 2015 Research progress of perovskite materials in photocatalysis- and photovoltaics-related energy conversion and environmental treatment *Chem. Soc. Rev.* **44** 5371–408
[42] Yang Y *et al* 2023 Synergistic surface activation during photocatalysis on perovskite derivative sites in heterojunction *Appl. Catal.* B **323** 122146
[43] Orak C, Atalay S, Ersöz G J S S and Technology 2017 Photocatalytic and photo-Fenton-like degradation of methylparaben on monolith-supported perovskite-type catalysts *Sep. Sci. Technol.* **52** 1310–20
[44] Huang C-W *et al* 2022 Solar-light-driven $LaFe_xNi_{1-x}O_3$ perovskite oxides for photocatalytic Fenton-like reaction to degrade organic pollutants *Beilstein J. Nanotechnol.* **13** 882–95
[45] Rojas-Cervantes M L and Castillejos E 2019 Perovskites as catalysts in advanced oxidation processes for wastewater treatment *Catalysts* **9** 230
[46] Shinichi E *et al* 2014 Fenton chemistry at aqueous interfaces *PNAS* **111** 623628
[47] Zhong X, Wu W, Jie H and Jiang F 2023 $La_2CoO_{4+\delta}$ perovskite-mediated peroxymonosulfate activation for the efficient degradation of bisphenol A *RSC Adv.* **13** 3193–203
[48] Tuna Ö and Bilgin Simsek E 2023 Promoted peroxymonosulfate activation into ferrite sites over perovskite for sunset yellow degradation: optimization parameters by response surface methodology *Opt. Mater.* **142** 114122